

Phase-separated symmetry-breaking vortex-lattice in a binary Bose-Einstein condensate

Sadhan K. Adhikari^{a,*}

^a*Instituto de Física Teórica, Universidade Estadual Paulista - UNESP, 01.140-070 São Paulo, São Paulo, Brazil*

Abstract

We study spontaneous-symmetry-breaking circularly-asymmetric phase separation of vortex lattices in a rapidly rotating harmonically-trapped quasi-two-dimensional (quasi-2D) binary Bose-Einstein condensate (BEC) with repulsive inter- and intra-species interactions. The phase separated vortex lattices of the components appear in different regions of space with no overlap between the vortices of the two components, which will permit an efficient experimental observation of such vortices and accurate study of the effect of atomic interaction on such vortex lattice. Such phase separation takes place when the intra-species interaction energies of the two components are equal or nearly equal with relatively strong inter-species repulsion. When the intra-species energies are equal, the two phase-separated vortex lattices have identical semicircular shapes with one being the parity conjugate of the other. When the intra-species energies are nearly equal, the phase separation is also complete but the vortex lattices have different shapes. We demonstrate our claim with a numerical solution of the mean-field Gross-Pitaevskii equation for a rapidly rotating quasi-2D binary BEC.

Keywords:

Binary Bose-Einstein condensate, Vortex-lattice formation, Gross-Pitaevskii equation, Spontaneous symmetry breaking

1. Introduction

Soon after the observation of ultra-dilute and ultra-cold trapped Bose-Einstein condensate (BEC) of alkali-metal atoms in a laboratory [1, 2], rapidly rotating trapped condensates were created and studied. A small number of vortices were created [3] for a small angular frequency of rotation Ω . Large vortex arrays were generated [4] with the increase of Ω . Similar to the vortices in super-fluid ^4He in a container, the vortices in trapped BEC also have quantized circulation: [5, 6] $\oint_C \mathbf{v} \cdot d\mathbf{r} = 2\pi\hbar l/m$, where C is a generic closed path, $\mathbf{v}(\mathbf{r}, t)$ is the super-fluid velocity field at the space point \mathbf{r} and time t , l is quantized integral angular momentum of an atom in units of \hbar in the trapped rotating BEC, and m is the mass of an atom. As Ω increases, it is energetically favorable to form a lattice of vortices of unit circulation each ($l = 1$) [6]. Consequently, a rapidly rotating trapped BEC generates a large number of vortices of

unit circulation arranged usually in a Abrikosov triangular lattice [4, 7]. The ultra-dilute trapped BEC is formed in the perturbative weak-coupling mean-field limit. This allows to study the formation of vortices in such a BEC by the mean-field Gross-Pitaevskii (GP) equation.

Vortex lattice formation in a trapped rotating binary BEC with a large number of vortices has also been observed [8, 9] and studied theoretically [10, 11]. There has also been study of vortex-lattice formation in a BEC along the weak-coupling to unitarity crossover [12] and in a rotating box trap [13]. The study of vortex lattices in a binary or a multi-component spinor BEC is interesting because the interplay between intra-species and inter-species interactions may lead to the formation of square [8, 14], stripe and honeycomb [15] vortex lattice, other than the standard Abrikosov triangular lattice [7]. In addition, there could be the formation of coreless vortices [16], vortices of fractional charge [17, 18], and phase-separated vortex lattices in multi-component non-spinor [19] spinor [11] and dipolar [14] BECs. The difficulty of experimental study of overlapping vortices in different components of a multi-component or a binary BEC

*Corresponding author

Email address: sk.adhikari@unesp.br (Sadhan K. Adhikari)

is monumental and despite great interest in the study of vortex lattices in a binary BEC [20, 21, 22, 23, 24, 25], this has highly limited such experimental studies [8, 9]. Hence for experimental study it will be highly desirable to have phase-separated vortex lattices in a binary BEC, where the vortices and component density of one component do not overlap with those of the other.

In a repulsive homogeneous BEC, phase separation takes place for [26]

$$\frac{g_1 g_2}{g_{12}^2} < 1, \quad (1)$$

where g_1 and g_2 are intra-species repulsion strengths for components 1 and 2, respectively, and g_{12} inter-species repulsion strength. This useful condition, although not rigorously valid in a trapped quasi-two-dimensional (quasi-2D) BEC, may provide an approximate guideline for phase separation. It is well-known that a phase separated vortex lattice in a rotating binary BEC can be generated by manipulating the parameters g_1, g_2 , and g_{12} [11, 26]. In this paper we identify the parameter domains leading to completely phase-separated vortex lattices in a rotating quasi-2D binary BEC so that the vortices of one component does not have any overlap with the matter density of the other component. We find that if g_1 and g_2 are equal and g_{12} is much larger than g_1 , then the phase separated components have the form of completely non-overlapping semi-circles lying opposite to each other spontaneously breaking the circular symmetry of the underlying Hamiltonian. In this case the vortex-lattice formation on the two component semi-circles has triangular symmetry with one component completely avoiding the other. If g_1 and g_2 are largely different and satisfy condition (1), one of the components lie on a circle at the center of the trap with the second component lying on a concentric circular annulus outside the first component maintaining the circular symmetry for a non-rotating binary BEC. In the case of a rotating binary BEC, although there will be phase-separated vortex lattices, the component densities will have irregular shape breaking the circular symmetry. If g_1 and g_2 are nearly equal and g_{12} much larger, the fully phase-separated components break circular symmetry and have different shapes. If such a phase-separated spontaneous-symmetry breaking binary BEC is subject to a rapid rotation, the generated vortex lattices maintain the same shape as the non-rotating binary BEC breaking the circular symmetry spontaneously. For $g_1 = g_2$, the phase-separated vortex lattices are dynamically stable. In this paper we will study numerically the generation of vortex lattices in these cases using the mean-field GP equation.

In Sec. II the mean-field model for a rapidly rotating binary BEC is presented. Under a tight trap in the transverse direction a quasi-2D version of the model is also given, which we use in the present study. The results of numerical calculation are shown in Sec. III. Finally, in Sec. IV we present a brief summary of our findings.

2. Mean-field model for a rapidly rotating binary BEC

We consider a binary rotating BEC interacting via inter- and intra-species interactions. The angular frequencies for the axially-symmetric harmonic trap along x, y and z directions are taken as $\omega_x = \omega_y = \omega$ and $\omega_z = \lambda\omega$, respectively. Now it is possible to make a binary BEC of two hyper-fine states of the same atomic species, such as ^{39}K and ^{87}Rb atoms. In such cases the masses of the two species are equal. Thus in this theoretical study we will take the masses of two species to be equal.

The study of a rapidly rotating binary BEC is conveniently performed in the rotating frame, where the generated vortex lattice is a stationary state [6], which can be obtained by the imaginary-time propagation method [27]. Such a dynamical equation in the rotating frame can be written if we note that the Hamiltonian in the rotating frame is given by $H = H_0 - \Omega l_z$, where H_0 is that in the laboratory frame, Ω is the angular frequency of rotation, l_z is the z component of angular momentum given by $l_z = i\hbar(y\partial/\partial x - x\partial/\partial y)$ [28]. However, if the rotational frequency Ω is increased beyond the trapping frequency ω , the rotating bosonic gas makes a quantum phase transition to a non-super-fluid state, where the validity of a mean-field description of the rotating bosonic gas is questionable [6]. Hence it is appropriate to limit this study to $\Omega < \omega$. With the inclusion of the extra rotational energy $-\Omega l_z$ in the Hamiltonian, the coupled GP equations for the binary BEC in the rotating frame for $\Omega < \omega$ can be written as [29]

$$i\hbar \frac{\partial \phi_1(\mathbf{r}, t)}{\partial t} = \left[-\frac{\hbar^2}{2m} \nabla^2 - \Omega l_z + \frac{1}{2} m \omega^2 (\rho^2 + \lambda^2 z^2) + \frac{4\pi\hbar^2}{m} \{a_1 N_1 |\phi_1(\mathbf{r}, t)|^2 + a_{12} N_2 |\phi_2(\mathbf{r}, t)|^2\} \right] \phi_1(\mathbf{r}, t), \quad (2)$$

$$i\hbar \frac{\partial \phi_2(\mathbf{r}, t)}{\partial t} = \left[-\frac{\hbar^2}{2m} \nabla^2 - \Omega l_z + \frac{1}{2} m \omega^2 (\rho^2 + \lambda^2 z^2) + \frac{4\pi\hbar^2}{m} \{a_2 N_2 |\phi_2(\mathbf{r}, t)|^2 + a_{12} N_1 |\phi_1(\mathbf{r}, t)|^2\} \right] \phi_2(\mathbf{r}, t), \quad (3)$$

where the two species of atoms of mass m each are denoted $i = 1, 2$, $\phi_i(\mathbf{r}, t)$ are the order parameters of the two components, N_i is the number of atoms in species i , $i = \sqrt{-1}$, $\mathbf{r} = \{x, y, z\}$, $\boldsymbol{\rho} = \{x, y\}$, $\rho^2 = x^2 + y^2$, a_i is the intra-species scattering length of species i , a_{12} is the inter-species scattering length. The functions ϕ_i are normalized as $\int d\mathbf{r} |\phi_i(\mathbf{r}, t)|^2 = 1$.

The following dimensionless form of Eqs. (2) and (3) can be obtained by the transformation of variables: $\mathbf{r}' = \mathbf{r}/l_0$, $l_0 \equiv \sqrt{\hbar/m\omega}$, $t' = t\omega$, $\phi'_i = \phi_i l_0^{3/2}$, $\Omega' = \Omega/\omega$, $l'_z = l_z/\hbar$ etc.:

$$i \frac{\partial \phi_1(\mathbf{r}, t)}{\partial t} = \left[-\frac{\nabla^2}{2} + \frac{1}{2}(\rho^2 + \lambda^2 z^2) - \Omega l_z + 4\pi N_1 a_1 |\phi_1|^2 + 4\pi a_{12} N_2 |\phi_2|^2 \right] \phi_1(\mathbf{r}, t), \quad (4)$$

$$i \frac{\partial \phi_2(\mathbf{r}, t)}{\partial t} = \left[-\frac{\nabla^2}{2} + \frac{1}{2}(\rho^2 + \lambda^2 z^2) - \Omega l_z + 4\pi N_2 a_2 |\phi_2|^2 + 4\pi a_{12} N_1 |\phi_1|^2 \right] \phi_2(\mathbf{r}, t), \quad (5)$$

where for simplicity we have dropped the prime from the transformed variables.

For a quasi-2D binary BEC in the $x - y$ plane under a strong trap along the z direction ($\lambda \gg 1$), the essential vortex dynamics will be confined to the $x - y$ plane with the z dependence playing a passive role. The wave functions can then be written as $\phi_i(\mathbf{r}, t) = \psi_i(\boldsymbol{\rho}, t)\Phi(z)$, where the function $\psi_i(\boldsymbol{\rho}, t)$ carries the essential vortex dynamics and $\Phi(z)$ is a normalizable Gaussian function. In this case the z dependence can be integrated out [30] and we have the following 2D equations

$$i \frac{\partial \psi_1(\boldsymbol{\rho}, t)}{\partial t} = \left[-\frac{\nabla^2}{2} + \frac{1}{2}\rho^2 - \Omega l_z + g_1 |\psi_1|^2 + g_{12} |\psi_2|^2 \right] \psi_1(\boldsymbol{\rho}, t), \quad (6)$$

$$i \frac{\partial \psi_2(\boldsymbol{\rho}, t)}{\partial t} = \left[-\frac{\nabla^2}{2} + \frac{1}{2}\rho^2 - \Omega l_z + g_2 |\psi_2|^2 + g_{21} |\psi_1|^2 \right] \psi_2(\boldsymbol{\rho}, t), \quad (7)$$

where $g_1 = 4\pi a_1 N_1 \sqrt{\lambda/2\pi}$, $g_2 = 4\pi a_2 N_2 \sqrt{\lambda/2\pi}$, $g_{12} = 4\pi a_{12} N_2 \sqrt{\lambda/2\pi}$, $g_{21} = 4\pi a_{12} N_1 \sqrt{\lambda/2\pi}$. In this study we will take $N_1 = N_2$ which will make $g_{12} = g_{21}$ maintaining the possibility $g_1 \neq g_2$ and consider $\Omega < 1$ [6].

The binary GP equations (6) and (7) can also be obtained using a variational procedure:

$$i \frac{\partial \psi_i(\boldsymbol{\rho}, t)}{\partial t} = \frac{\delta E}{\delta \psi_i^*(\boldsymbol{\rho}, t)} \quad (8)$$

with the following energy functional in the rotating

frame:

$$E[\psi] = \int d\boldsymbol{\rho} \left[\sum_i \frac{1}{2} \left(|\nabla \psi_i|^2 + \rho^2 |\psi_i|^2 + g_i |\psi_i|^4 - 2\psi_i^* l_z \Omega \psi_i \right) + g_{12} |\psi_1|^2 |\psi_2|^2 \right]. \quad (9)$$

We note that the rotational energy $-\int d\boldsymbol{\rho} \psi_i^* l_z \Omega \psi_i$ is negative. Hence the energy E in the rotating frame will decrease with the increase of angular frequency of rotation. All other contributions to energy (9) are positive. Hence in the perturbative limit of small Ω , the total energy will be positive with the energy decreasing linearly with Ω . For very large Ω ($\Omega < 1$, $\Omega \rightarrow 1$), the contribution of the rotational energy will be proportional to Ω^2 [31] and the total energy will decrease quadratically with Ω , viz. Fig. 5(b) below.

3. Numerical Results

The quasi-2D binary mean-field equations (6) and (7) cannot be solved analytically and different numerical methods, such as the split time-step Crank-Nicolson method [27, 32] or the pseudo-spectral method [33], can be employed for their solution. Apart from the basic C and FORTRAN programs for solving the GP equation [27], their open multi-processing (OMP) versions [32] are also available and one should use the appropriate one. The OMP versions reduce the execution time significantly in a multi-core multi-processing computer. These OMP programs have recently been adapted to simulate the vortex lattice in a rapidly rotating BEC [34] and we use these in this study. Here we solve Eqs. (6) and (7) by the split time-step Crank-Nicolson discretization scheme using a space step of 0.05 and a time step of 0.0002 for imaginary-time simulation and 0.0001 for real-time simulation. The imaginary-time simulation is performed with a localized initial state modulated by a random phase at each space grid point as in Refs. [13, 34]. The random phase modulation allows an efficient generation of vortex lattice independent of the algebraic form of the initial state. The real-time simulation is performed with the converged imaginary-time wave function as the initial state.

In this paper, without considering a specific atom, we will present the results in dimensionless units for different sets of parameters: $\Omega, g_1, g_2, g_{12}(=g_{21})$. In the phenomenology of a specific atom, the parameters g_1, g_2, g_{12} can be varied experimentally through a variation of the underlying intra- and inter-species scattering lengths by the Feshbach resonance technique [35].

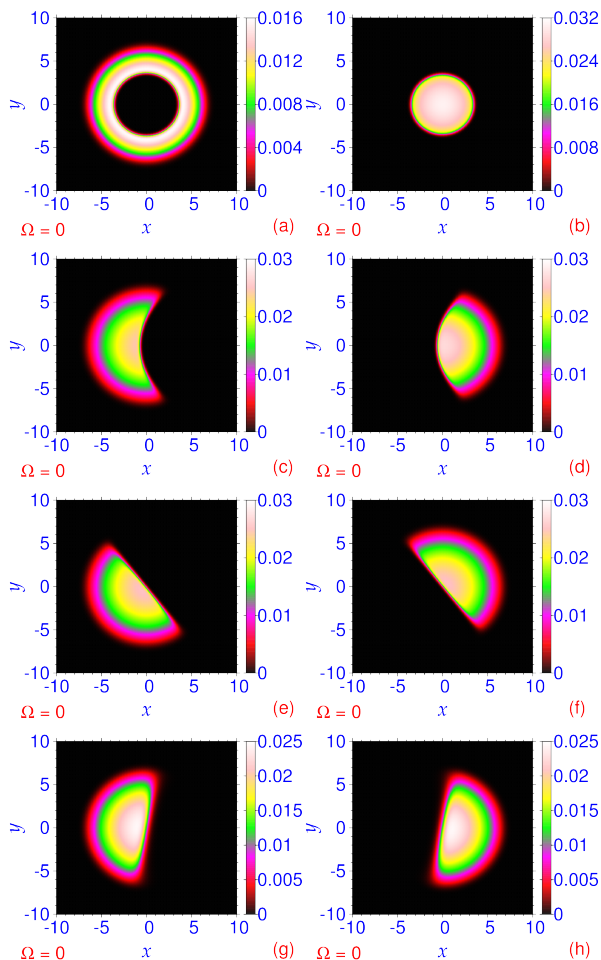


Figure 1: Phase separation in a non-rotating ($\Omega = 0$) binary BEC from a contour plot of 2D densities ($|\psi_i|^2$): (a) first and (b) second components for $g_{12} = 2000, g_1 = 1000, g_2 = 700$, (c) first and (d) second components for $g_{12} = 2000, g_1 = 1000, g_2 = 900$ (e) first and (f) second components for $g_{12} = 2000, g_1 = g_2 = 1000$, (g) first and (h) second components for $g_{12} = 1100, g_1 = g_2 = 1000$. All quantities plotted in this and following figures are dimensionless.

First we demonstrate a phase separation in a fully repulsive ($g_i, g_{12} > 0$) non-rotating binary BEC ($\Omega = 0$). We find that a phase separation generally follows the condition (1) for $g_1 \approx g_2$; so that $g_{12} > g_1, g_2$. For our purpose, we consider $g_1 = 1000, g_{12} = 2000$ and $g_2 =$ (i) 700, (ii) 900, (iii) 1000, and (iv) $g_1 = g_2 = 1000$ with $g_{12} = 1100$. The result of phase separation is shown in Figs. 1(a)-(h), where we plot density of the two components. In case (i) $g_1 = 1000$ and $g_2 = 700$ are quite different maintaining $g_{12} = 2000$ much larger than g_1 and g_2 and phase separation maintains circular symmetry as shown in Figs. 1(a)-(b). As $g_2 = 900$

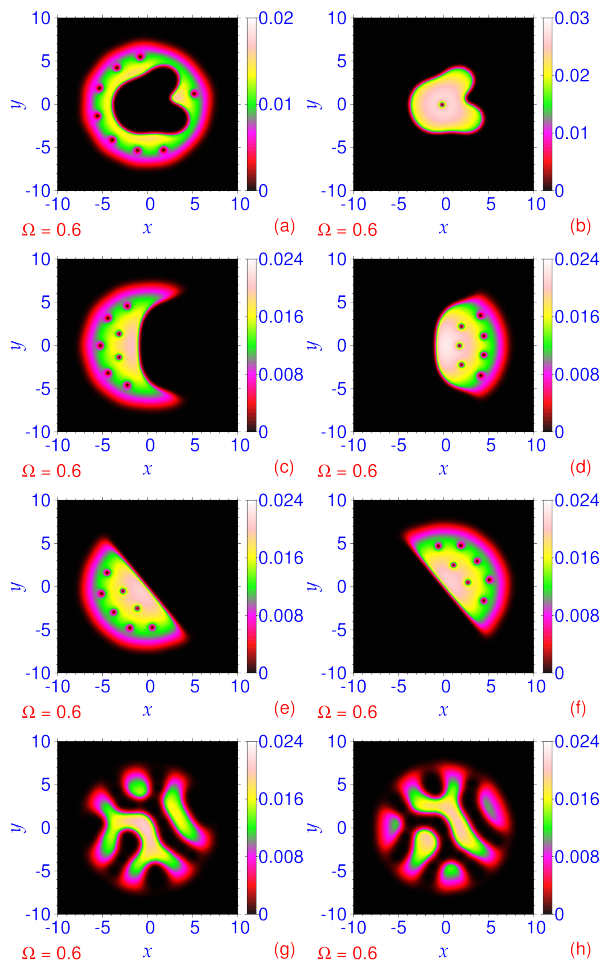


Figure 2: Phase-separated vortex lattices in a rapidly rotating binary BEC with $\Omega = 0.6$ from a contour plot of 2D densities ($|\psi_i|^2$): (a) first and (b) second components for $g_1 = 1000, g_2 = 700, g_{12} = 2000$, (c) first and (d) second components for $g_1 = 1000, g_2 = 900, g_{12} = 2000$, (e) first and (f) second components for $g_1 = g_2 = 1000, g_{12} = 2000$, (g) first and (h) second components for $g_1 = g_2 = 1000, g_{12} = 1100$, corresponding to the non-rotating BECs shown in Fig. 1(a)-(h), respectively.

approaches $g_1 = 1000$ in case (ii), the phase separation spontaneously breaks the circular symmetry of the Hamiltonian as shown in Figs. 1(c)-(d). In case (iii), $g_1 = g_2 = 1000$ and the phase separation breaks the circular symmetry, viz. Figs. 1(e)-(f), with the density of component 1 being the parity conjugate of the density of component 2. Finally, in case (iv) $g_{12} = 1100$ approaches $g_1 = g_2 = 1000$ consistent with condition (1), maintaining a parity symmetric phase separation. In this paper, we will be interested in robust spontaneous-symmetry breaking phase separated vortex lattices without overlap between component densities, which is of

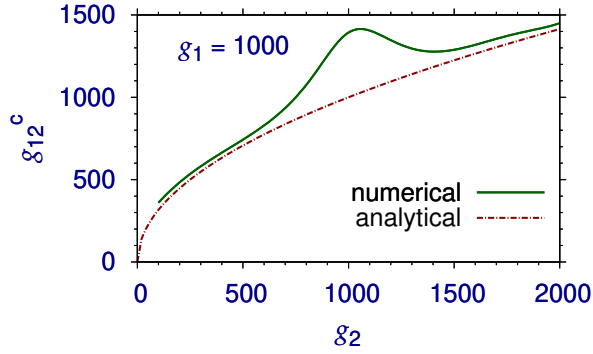


Figure 3: The numerical g_{12}^c versus g_2 for $g_1 = 1000$ and its analytical estimate $g_{12}^c = \sqrt{g_1 g_2}$ from Eq. (1). The numerical estimate is found to be independent of the angular frequency of rotation Ω .

great experimental interest. Hence cases (ii), (iii), and (iv) seem to be attractive candidates and we next study the generation of vortex lattices in the cases displayed in Fig. 1.

In Figs. 2(a)-(h) we plot the component densities of a rotating binary BEC with angular frequency of rotation $\Omega = 0.6$ with same interaction parameters g_1, g_2, g_{12} as the non-rotating BECs considered in Figs. 1(a)-(h). The case (i) illustrated in Figs. 2(a)-(b) breaks the circular symmetry generating an irregular shape of the components and hence an irregular arrangement of vortices and we will not study this case in detail. In the non-rotating BEC with same parameters, the component densities maintain circular symmetry, viz. Figs. 1(a)-(b). In case (ii) displayed in Figs. 2(c)-(d) the rotating BEC has density profile quite similar to the non-rotating BEC of Figs. 1(c)-(d). The same is true in Figs. 2(e)-(f) when compared with Figs. 1(e)-(f). Nevertheless, the arrangement of vortices in Figs. 2(c)-(f) is very ordered with a definite (triangular) symmetry. In Figs. 2(g)-(h), quite surprisingly, the phase separation found in the non-rotating BEC of Figs. 1(g)-(h) has disappeared generating two component BECs occupying the whole region of space. Moreover, no visible vortices are found in Figs. 2(g)-(h). This type of density distribution is called vortex sheet structure which has been found before in binary BECs [15, 24]. This case is not of interest of the present study. In the following we will study vortex lattice generation in cases (ii) and (iii) in some detail with a triangular arrangement of vortices in the components and with complete phase separation of the density of the two components.

First we study how the number of vortices and energy evolve with the increase of angular frequency of rota-

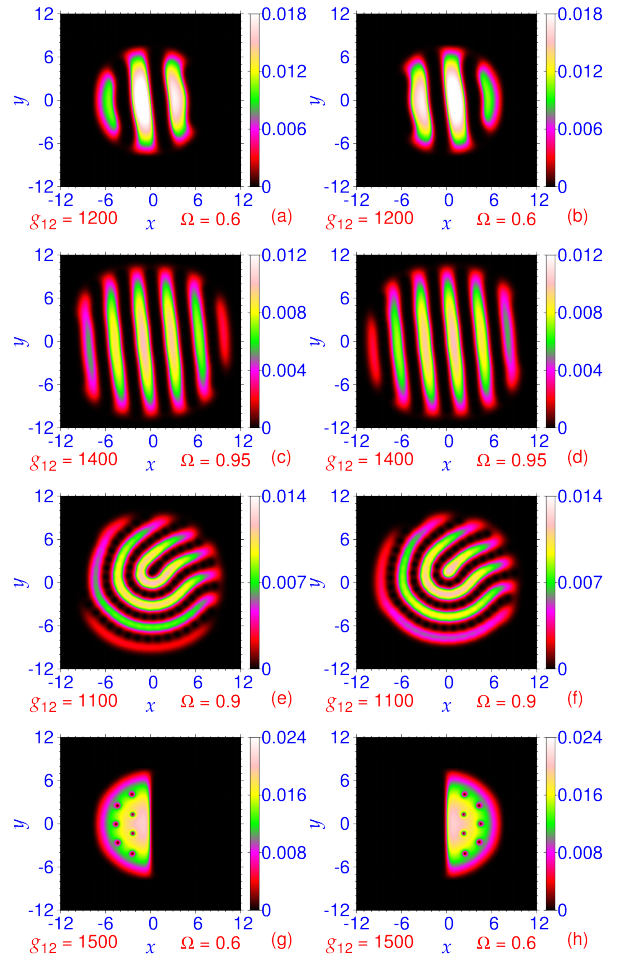


Figure 4: Contourplot of 2D density of a rapidly rotating binary BEC for $g_1 = g_2 = 1000$. (a) first and (b) second components for $g_{12} = 1200, \Omega = 0.6$; (c) first and (d) second components for $g_{12} = 1400, \Omega = 0.95$; (e) first and (f) second components for $g_{12} = 1100, \Omega = 0.9$; (g) first and (h) second components for $g_{12} = 1500, \Omega = 0.6$.

tion Ω . For this purpose we consider the symmetric case $g_1 = g_2 = 1000$ with $g_{12} = 2000$. We consider a large g_{12} as for a large g_{12} the phase separation is very stable leading to a ground state with phase-separated vortex lattice. For $g_{12} \gtrsim g_1 = g_2$, there is phase separation, but the ground state has a phase-separated sheet structure [15, 24], viz. Fig. 2(g)-(h). The fully phase-separated states in this case with $g_1 = g_2 = 1000, g_{12} = 1100$, similar to those in Figs. 2(e)-(f), are excited states of higher energy. As g_{12} increases, the difference of energy between these two types of states reduce and beyond a certain critical g_{12}^c the fully phase-separated states become the ground state which can be studied experimentally. In Fig. 3 we plot the numerically computed g_{12}^c versus

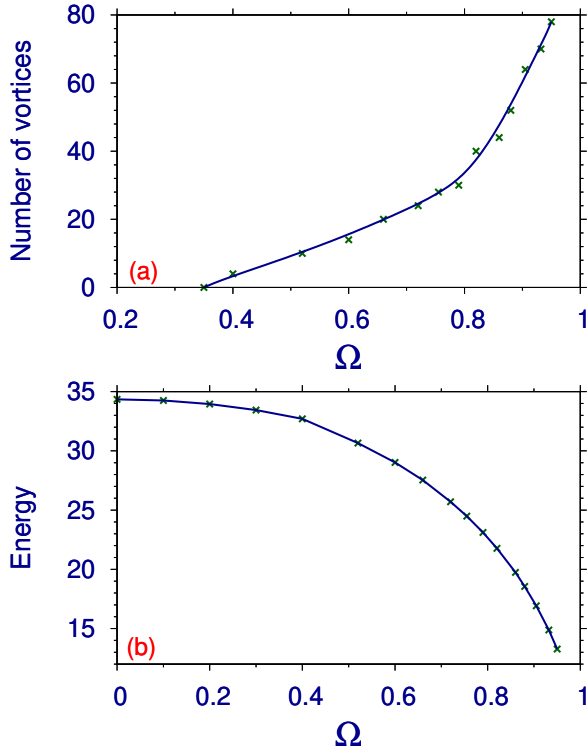


Figure 5: (a) Number of vortices and (b) energy in the rotating frame (9) for a rapidly rotating quasi-2D binary BEC with $g_1 = g_2 = 1000$, $g_{12} = 2000$ versus angular frequency of rotation Ω . The crosses are the actual points obtained numerically whereas the lines are shown to guide the eye.

g_2 for a fixed $g_1 = 1000$ and $\Omega = 0.6$ and compare with the analytical result $g_{12}^c \equiv \sqrt{g_1 g_2} = \sqrt{1000 g_2}$, signaling a phase separation of a uniform (non-rotating) binary mixture, obtained from Eq. (1). The numerical critical value g_{12}^c is found to be independent of Ω (< 1). For values of g_{12} larger than the numerical g_{12}^c , phase separated vortex lattice is obtained. From Fig. 3 we find that the formation of phase separated vortex lattice is most problematic for $g_1 = g_2$ and we study the formation of phase separated vortex lattice for this case in some details. For values of g_{12} between the numerical and analytical estimates of g_{12}^c , either straight stripe structure, viz. Fig. 4(a)-(d), or sheet or bent stripe structure, viz. Fig. 2(g)-(h) and Fig. 4(e)-(f), is formed for $g_1 = g_2 = 1000$ [24]. Only for g_{12} larger than its numerically obtained critical value, phase separated vortex lattice is formed as shown in Fig. 4(g)-(h). We find that the size and the number of stripes increase as the angular frequency of rotation is increased, viz. Fig. 4(a)-(d). The straight stripes become bent for smaller g_{12} , viz. Fig. 4(e)-(f), which change to sheet structure for small angular fre-

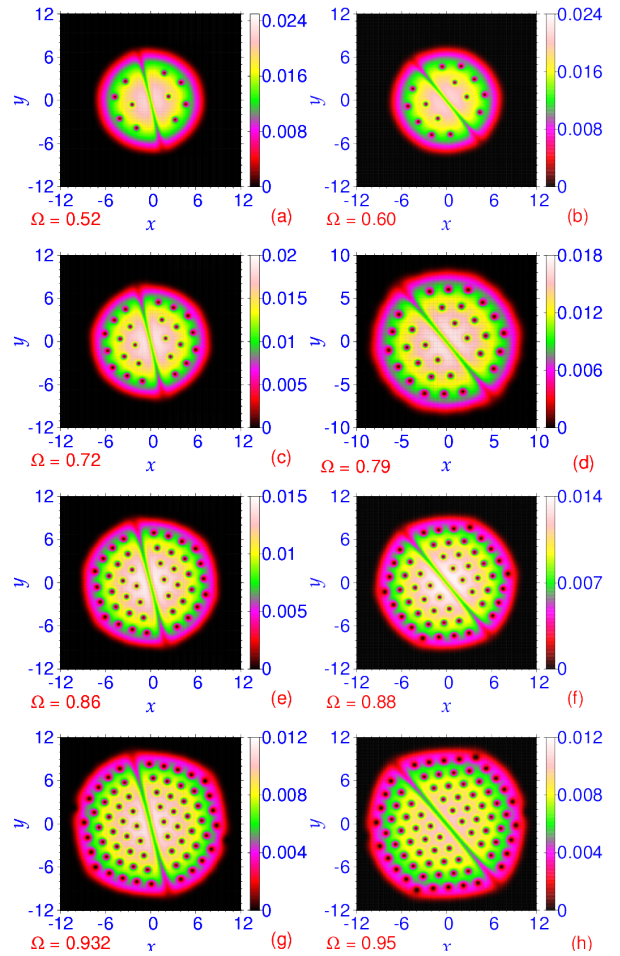


Figure 6: First and second components of a rotating binary BEC with angular frequency of rotation $\Omega =$ (a) 0.52, (b) 0.6, (c) 0.72, (d) 0.79, (e) 0.86, (f) 0.88, (g) 0.932, and (h) 0.95 with the respective number of vortices 10, 14, 24, 30, 44, 52, 70, 80. Other parameters are $g_1 = g_2 = 1000$, $g_{12} = g_{21} = 2000$.

quency Ω , viz. Fig. 2(g)-(h).

We study the generation of vortex lattice for $g_1 = g_2 = 1000$ with $g_{12} = 2000$. The fully phase-separated states are the ground states for all Ω . In Figs. 5(a)-(b) we plot the number of vortices and energy in the rotating frame (9) versus Ω . As expected, the number of vortices increase with Ω and energy decreases as Ω is increased. The energy decreases as the contribution of the rotational energy $-\Omega l_z$ in the expression for energy is negative. For small Ω , in the perturbative limit, this contribution is linearly proportional to $-\Omega$. But as Ω increases, the number of vortices increase rapidly and in that non-perturbative domain the rotational energy behaves as Ω^2 [6]. In Fig. 5(b), this transition from linear

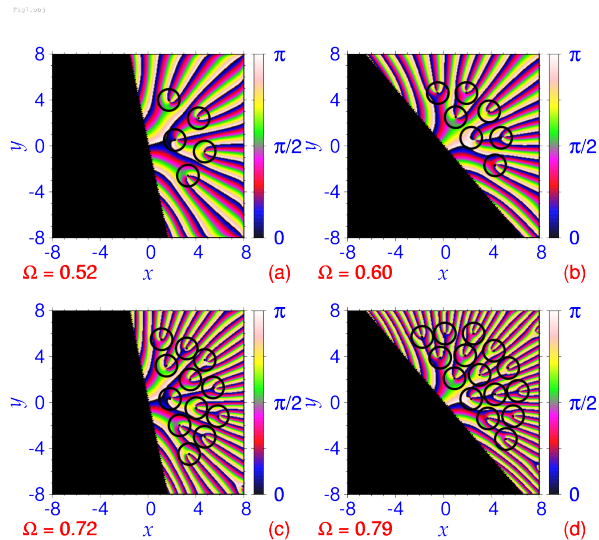


Figure 7: (a)-(d) A contour plot of the phase of the second component of the wave function on the condensate surface corresponding to the vortex lattice shown in Figs. 6(a)-(d), respectively. The position of the vortices are marked by a closed circular contour.

to quadratic dependence on Ω is seen as Ω increases.

The generation of vortex lattice in the symmetric case $g_1 = g_2$ reveals very interesting features. The study is performed with the parameters $g_1 = g_2 = 1000, g_{12} = 2000$. Robust triangular vortex lattice is generated in this case on two completely separated semicircular components as shown in Figs. 2(e)-(f). The generated vortex lattices for $\Omega = 0.52, 0.60, 0.72, 0.79, 0.86, 0.88, 0.932$, and 0.95 are shown in Figs. 6(a)-(h), respectively. As the phase separation is complete in this case we have displayed the vortex lattices of the two components of the binary BEC in the same plot. The separation between the two components can be clearly seen in this figure in a domain of low density between the two components. Comparing Figs. 2(e)-(f) on the one hand and Fig. 6(b) on the other, we find that Fig. 6(b) provides a more concise illustration of the binary vortex lattice. For the sake of convergence of the numerical scheme, we used a larger domain of space in the numerical calculation than the space domain shown in the plots of Fig. 6. The maximum density of the condensate in these plots reduce with the increase of Ω as can be seen in this figure. With the increase of Ω , due to increased centrifugal repulsion, the binary condensate occupies a larger space domain thus reducing the maximum density. Another remarkable feature of the vortex lattice generation in Fig. 6 is the robust accurate triangular lattice formation in plots

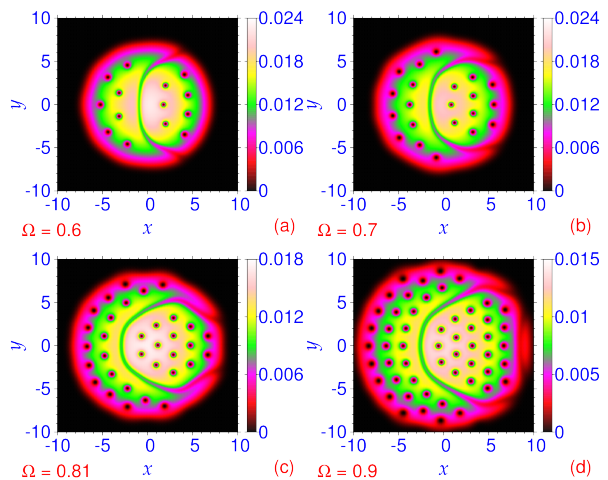


Figure 8: First and second components of a rotating binary BEC with angular frequency of rotation $\Omega =$ (a) 0.6, (b) 0.7, (c) 0.81, and (d) 0.9, and $g_1 = 1000, g_2 = 900, g_{12} = g_{21} = 2000$ with the respective number of vortices 14 (7+7), 21 (11+10), 33 (19+14), 54 (31+23). The vortex lattice of the first component with larger interaction strength ($g_1 = 1000$) than that of the second component ($g_2 = 900$) in on the left side of each plot and that of the second component is on the right side.

(e)-(h).

To demonstrate that all spots in density of Fig. 6 correspond to vortices, we display the phase of the wave function $\arctan[\Im(\psi_i)/\Re(\psi_i)]$ on the condensate surface in Figs. 7(a)-(d) corresponding to the vortex lattice of Figs. 6(a)-(d), where \Im and \Re are imaginary and real parts. Quantum vortices in a rotating super-fluid have unit circulation ($l = 1$) each. In a closed path around a vortex of unit angular momentum, the phase changes by 2π . In Figs. 7 the phase over the second component is shown and the position of the vortices are indicated by a closed contour. A careful survey of these phases reveals that the accumulated phase of the wave function around the clockwise contour is always 2π corresponding to a vortex of unit angular momentum. It is never -2π corresponding to an anti-vortex or multiples of 2π corresponding to a vortex of multiple angular momentum ($l > 1$).

Next we consider the generation of vortex lattice in the asymmetric case $g_1 = 1000 \neq g_2 = 900, g_{12} = 2000$ briefly illustrated in Fig. 2(c)-(d) and Fig. 8(a) for $\Omega = 0.6$. The same for $\Omega = 0.7, 0.81$ and 0.9 are displayed in Fig. 8 (b)-(d), respectively. In this case there is a complete phase separation, but the sizes (extensions) of the components are different. Also, as before, it is appropriate to display the density of both components in the same plot, where it is possible to identify the two

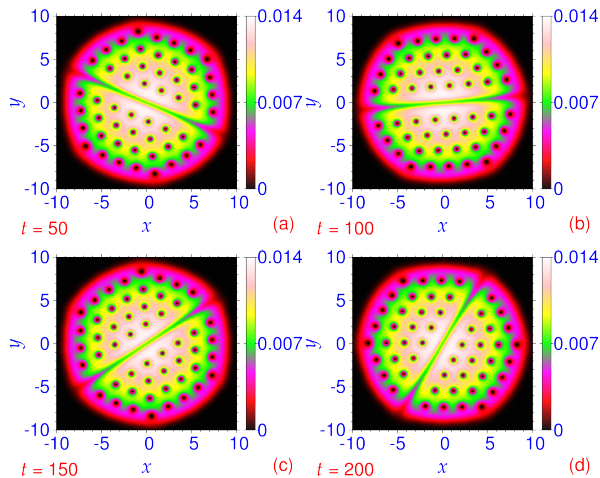


Figure 9: Dynamical evolution of vortex lattice of a rotating binary BEC, displayed in Fig. 6(f), during real-time propagation for 200 units of time using the corresponding imaginary-time wave function as input, at times (a) $t = 50$, (b) $t = 100$, (c) $t = 150$, and (d) $t = 200$. During real-time propagation the angular frequency of rotation Ω was changed at $t = 0$ from the imaginary-time value of $\Omega = 0.88$ to 0.89 .

components clearly. The maximum density of the condensate decreases with the increase of Ω and the number of vortices increases with Ω . The filling of the vortices on the components is only approximately of triangular geometry because of the irregular shape of the components of the condensates.

The dynamical stability of the vortex lattices of the rotating binary BEC is tested next. For this purpose we subject the vortex-lattice state of the rotating BEC to real-time evolution during a large interval of time, after slightly changing the angular frequency of rotation Ω at $t = 0$. The vortex lattice will be destroyed after some time, if the underlying BEC wave function were dynamically unstable. We consider real-time propagation of the vortex lattice exhibited in Fig. 6(f) for $g_1 = g_2 = 1000$, $g_{12} = 2000$ after changing Ω from 0.88 to 0.89 at $t = 0$. The subsequent evolution of the vortex lattice is displayed in Fig. 9 at (a) $t = 50$, (b) $t = 100$, (c) $t = 150$, and (d) $t = 200$. The robust nature of the snapshots of vortex lattice during real-time evolution upon a small perturbation, as exhibited in Fig. 9, demonstrates the dynamical stability of the vortex lattice in the quasi-2D rotating binary condensate.

4. Summary and Discussion

We have studied the generation of spontaneous symmetry-breaking completely phase-separated

circularly-asymmetric vortex lattices in a harmonically-trapped repulsive quasi-2D binary BEC. In the examples studied in this paper there is no overlap between the component densities of the BEC so that vortex lattices of the two components are formed in different regions of space, which is of great phenomenological interest. This will facilitate the experimental study of the vortex lattices of the two components. Such vortex-lattice structure is generated when the quantity in Eq. (1) is much smaller than unity, e.g., $g_1 g_2 / g_{12}^2 \lesssim 0.75$ or so. For larger values of this ratio, although there could be a phase separation for a non-rotating binary BEC, overlapping sheet structure [15, 24] appear for a rotating binary BEC, viz. Figs. 2(g)-(h). In this study we fixed this ratio as: $g_1 g_2 / g_{12}^2 \approx 0.5$. We considered both symmetric and asymmetric cases of intra-species interaction strengths: $g_1 = g_2$ and $g_1 \neq g_2$, respectively. In the former case the vortex lattices of the two components lie on fully separated semicircles which are parity conjugates of each other. In the asymmetric case, although the phase separation is complete, the shapes of the two components are different. Of these two, we demonstrated dynamical stability of the symmetric vortex lattice by long-time real-time simulation upon a small change in the angular frequency of rotation, viz. Fig. 9. The asymmetric vortex lattice is found to be only weakly stable. With present experimental know-how these phase-separated vortex lattices can be generated and studied in a laboratory.

Acknowledgements

SKA thanks the Fundação de Amparo à Pesquisa do Estado de São Paulo (Brazil) (Project: 2016/01343-7) and the Conselho Nacional de Desenvolvimento Científico e Tecnológico (Brazil) (Project: 303280/2014-0) for partial support.

References

- [1] M. H. Anderson, J. R. Ensher, M. R. Matthews, C. E. Wieman, and E. A. Cornell, *Science* 269 (1995) 198.
- [2] K. B. Davis, M. -O. Mewes, M. R. Andrews, N. J. van Druten, D. S. Durfee, D. M. Kurn, and W. Ketterle, *Phys. Rev. Lett.* 75 (1995) 3969.
- [3] K. W. Madison, F. Chevy, W. Wohlleben, and J. Dalibard, *Phys. Rev. Lett.* 84 (2000) 806; M. R. Matthews, B. P. Anderson, P. C. Haljan, D. S. Hall, M. J. Holland, J. E. Williams, C. E. Wieman, and E. A. Cornell, *Phys. Rev. Lett.* 83 (1999) 3358.
- [4] J. R. Abo-Shaer, C. Raman, J. M. Vogels, and W. Ketterle, *Science* 292 (2001) 476; P. C. Haljan, B. P. Anderson, I. Coddington, and E. A. Cornell, *Phys. Rev. Lett.* 86 (2001) 2922.

- [5] E. B. Sonin, *Dynamics of Quantised Vortices in Superfluids* (Cambridge University Press, Cambridge, 2016).
- [6] A. L. Fetter, *Rev. Mod. Phys.* 81 (2009) 647.
- [7] A. A. Abrikosov, *Zh. Eksp. Teor. Fiz.* 32 (1957) 1442; [Eng. Transla. *Sov. Phys.-JETP* 5 (1957) 1174.]
- [8] V. Schweikhard, I. Coddington, P. Engels, S. Tung, E. A. Cornell, *Phys. Rev. Lett.* 93 (2004) 210403.
- [9] D. S. Hall, M. R. Matthews, J. R. Ensher, C. E. Wieman, E. A. Cornell, *Phys. Rev. Lett.* 81 (1998) 1539.
- [10] H. Wang, *J. Sci. Comput.* 38 (2009) 149;
Y. Zhanga, W. Bao, H. Li, *Physica D* 234 (2007) 49;
C.-H. Hsueh, T.-L. Horng, S.-C. Gou, W. C. Wu, *Phys. Rev. A* 84 (2011) 023610;
Q. Zhao, *Int. J. Mod. Phys. B* 33 (2019) 1950080;
X.-F. Zhang, L. Wen, C.-Q. Dai, R.-F. Dong, H.-F. Jiang, H. Chang, S.-G. Zhang, *Scientific Rep.* 6 (2016) 19380.
- [11] P. Mason, A. Aftalion, *Phys. Rev. A* 84 (2011) 033611;
A. Aftalion, P. Mason, J. Wei, *Phys. Rev. A* 85 (2012) 033614.
- [12] S. K. Adhikari, L. Salasnich, *Scientific Rep.* 8 (2018) 8825.
- [13] S. K. Adhikari, *J. Phys.: Condens. Matter* 31 (2019) 275401.
- [14] R. K. Kumar, L. Tomio, B. A. Malomed, A. Gammal, *Phys. Rev. A* 96 (2017) 063624;
R. K. Kumar, L. Tomio, A. Gammal, *Phys. Rev. A* 99 (2019) 043606;
N. Ghazanfari, A. Keleş, M. Ö. Oktel, *Phys. Rev. A* 89 (2014) 025601.
- [15] K. Kasamatsu, K. Sakashita, *Phys. Rev. A* 97 (2018) 053622.
- [16] A. E. Leanhardt, Y. Shin, D. Kielpinski, D. E. Pritchard, W. Ketterle, *Phys. Rev. Lett.* 90 (2003) 140403.
- [17] S.-W. Su, C.-H. Hsueh, I.-Kang Liu, T.-L. Horng, Y.-C. Tsai, S.-C. Gou, W. M. Liu, *Phys. Rev. A* 84 (2011) 023601.
- [18] M. Cipriani, M. Nitta, *Phys. Rev. Lett.* 111 (2013) 170401.
- [19] S. K. Adhikari, *Commun. Nonlinear Sci. Numer. Simulat.* 71 (2019) 212.
- [20] E. J. Mueller, T.-L. Ho, *Phys. Rev. Lett.* 88 (2002) 180403.
- [21] R. Barnett, G. Refael, M. A. Porter, H. P. Buchler, *New J. Phys.* 10 (2008) 043030;
Z. Chen, Y. Li, N. P. Proukakis, B. A. Malomed, *New J. Phys.* 21 (2019) 073058.
- [22] R. Wei, E. Mueller, *Phys. Rev. A* 84 (2011) 063611.
- [23] P. Kuopanportti, J. A. M. Huhtamäki, M. Möttönen, *Phys. Rev. A* 85 (2012) 043613.
- [24] K. Kasamatsu, M. Tsubota, *Phys. Rev. A* 79 (2009) 023606; K. Kasamatsu, M. Tsubota, M. Ueda, *Phys. Rev. Lett.* 91 (2003) 150406.
- [25] K. Kasamatsu, M. Tsubota, M. Ueda, *Int. J. Mod. Phys. B* 19 (2005) 1835.
- [26] See, for example, V.P. Mineev, *Zh. Eksp. Teor. Fiz.* 67 (1974) 263; [Eng. Transla. V.P. Mineev, *Sov. Phys.-JETP* 40 (1975) 132];
E. Timmermans, *Phys. Rev. Lett.* 81 (1998) 5718;
K. L. Lee, N. B. Jorgensen, I.-K. Liu, L. Wacker, J. J. Arlt, N. P. Proukakis, *Phys. Rev. A* 94 (2016) 013602.
- [27] P. Muruganandam, S. K. Adhikari, *Comput. Phys. Commun.* 180 (2009) 1888;
D. Vudragović, I. Vidanović, A. Balaž, P. Muruganandam, S. K. Adhikari, *Comput. Phys. Commun.* 183 (2012) 2021.
- [28] L. D. Landau, E. M. Lifshitz, *Mechanics* (Pergamon Press, Oxford, 1960), section 39.
- [29] A. L. Fetter, B. Jackson, S. Stringari, *Phys. Rev. A* 71 (2005) 013605.
- [30] L. Salasnich, A. Parola, L. Reatto, *Phys. Rev. A* 65 (2002) 043614.
- [31] Sec. IV of Ref. [6].
- [32] L. E. Young-S., P. Muruganandam, S. K. Adhikari, V. Lončar, D. Vudragović, A. Balaž, *Comput. Phys. Commun.* 220 (2017) 503;
L. E. Young-S., D. Vudragović, P. Muruganandam, S. K. Adhikari, A. Balaž, *Comput. Phys. Commun.* 204 (2016) 209;
B. Satačić, V. Slavnić, A. Belić, A. Balaž, P. Muruganandam, S. K. Adhikari, *Comput. Phys. Commun.* 200 (2016) 411.
- [33] P. Muruganandam, S. K. Adhikari, *J. Phys. B* 36 (2003) 2501.
- [34] R. Kishor Kumar, V. Lončar, P. Muruganandam, S. K. Adhikari, A. Balaž, *Comput. Phys. Commun.* 240 (2019) 74.
- [35] S. Inouye, M. R. Andrews, J. Stenger, H.-J. Miesner, D. M. Stamper-Kurn, W. Ketterle, *Nature* 392 (1998) 151.